Supporting Information

Benzene Probes in Molecular Dynamics Simulations Reveal Novel Binding Sites for Ligand Design

Yaw Sing Tan,[†] Judith Reeks,[§] Christopher J. Brown,[⊥] Dawn Thean,[⊥] Fernando Jose Ferrer Gago,[⊥] Tsz Ying Yuen,[‖] Eunice Tze Leng Goh,[∇] Xue Er Cheryl Lee,[⊥] Claire E. Jennings,[§] Thomas L. Joseph,[†] Rajamani Lakshminarayanan,[∇] David P. Lane,[*,⊥] Martin E. M. Noble,[*,§] Chandra S. Verma[*,†,#,○]

[†]Bioinformatics Institute, Agency for Science, Technology and Research (A*STAR), 30 Biopolis Street, #07-01 Matrix, Singapore 138671

[§]Northern Institute for Cancer Research, Newcastle University, Framlington Place, Newcastle upon Tyne, NE2 4HH, U.K.

[⊥]p53 Laboratory, A*STAR, 8A Biomedical Grove, #06-04/05 Neuros/Immunos, Singapore 138648

[‖]Institute of Chemical & Engineering Sciences, A*STAR, 8 Biomedical Grove, #07-01 Neuros, Singapore 138665

[∇]Singapore Eye Research Institute, 11 Third Hospital Avenue, Singapore 168751

[#]Department of Biological Sciences, National University of Singapore, 14 Science Drive 4, Singapore 117543

[○]School of Biological Sciences, Nanyang Technological University, 60 Nanyang Drive, Singapore 637551

Contents

1. Computational modeling

Preparation of structures

The crystal structure of human MDM2 (residues 25-109) bound to the p53 transactivation domain peptide (residues 17-29) was obtained from the Protein Data Bank (PDB)[1] and used as the initial structure for molecular dynamics (MD) simulations (PDB code 1YCR).[2] The initial structure of the MDM2–sMTide-02 complex was generated by first extracting the phage display peptide PMI (TSFAEYWNLLSP) from the PDB structure 3EQS[3] and modeling it onto the MDM2 structure from 1YCR. PMI was then modified into the stapled peptide sMTide-02 (Ac-TSF**R$_8$**EYWALL**S$_5$**-NH$_2$)[4] by using the LEaP module of AMBER 11[5] to form the trans carbon-carbon double bond between the **R$_8$** and **S$_5$** residues. **R$_8$** represents an (R)-2-(7'-octenyl)alanine residue while **S$_5$** represents an (S)-2-(4'-pentenyl)alanine residue. Acetyl and N-methyl groups were used to cap the N- and C- termini of MDM2 respectively, while the peptides were capped by acetyl and amide groups. PDB2PQR[6] was used to determine the protonation states of residues and add missing hydrogen atoms. The LEaP module in the AMBER 11 package was then used to solvate each system with TIP3P water molecules[7] in a periodic truncated octahedron box, such that its walls were at least 9 Å away from the protein, and for neutralization of charges with either sodium or chloride ions.

Molecular dynamics

Using different initial atomic velocities and seeds for the pseudorandom number generator, two independent explicit-solvent MD simulations were carried out on each of the MDM2–p53 and MDM2–sMTide-02 complexes. Energy minimizations and MD simulations were performed with the sander and PMEMD modules of AMBER 11, using the ff99SB-ILDN force field.[8] The R$_8$ and S$_5$ residues were described by both the ff99SB-ILDN and generalized AMBER force fields (GAFF).[9] Atomic charges for R$_8$ and S$_5$ (Tables S1 and S2 respectively) were derived using the R.E.D. Server,[10] by fitting restrained electrostatic potential (RESP) charges[11] to a molecular electrostatic potential (MEP) computed by the Gaussian 09 program[12] at the HF/6-31G* level of theory. All bonds involving hydrogen atoms were constrained by the SHAKE algorithm,[13] allowing for a time step of 2 fs. Nonbonded interactions were truncated at 9 Å, and the particle mesh Ewald method[14] was used to account for long range electrostatic interactions under periodic boundary conditions.

Weak harmonic positional restraints with a force constant of 2.0 kcal mol^{-1} $Å^{-2}$ were placed on the protein and peptide non-hydrogen atoms during the minimization and initial equilibration steps. Energy minimization was carried out using the steepest descent algorithm for 500 steps, followed by the conjugate gradient algorithm for another 500 steps. The system was then heated gradually to 300 K over 50 ps at constant volume before equilibration at a constant pressure of 1 atm for another 50 ps. Subsequent unrestrained equilibration (2 ns) and production (50 ns) runs were carried out at 300 K using a Langevin thermostat[15] with a collision frequency of 2 ps^{-1}, and 1 atm using a Berendsen barostat[16] with a pressure relaxation time of 2 ps.

Ligand-mapping MD simulations

Ligand-mapping MD (LMMD) simulations were carried out on both unbound and p53-bound MDM2. For each set of simulations, 10 different distributions of benzenes around the protein were created using Packmol.[17] The LEaP module in the AMBER 11 package was then used to solvate each system with TIP3P water molecules in a periodic truncated octahedron box, such that its walls were at least 9 Å away from the protein, and for neutralization of charges with either sodium or chloride ions, resulting in a final benzene concentration of ~0.2 M. Minimization, equilibration and production (5 ns) MD simulations were carried out as described above for the MDM2 complexes, for a cumulative sampling time of 50 ns. The GAFF[9] force field was used to describe the benzenes during the simulations. Atomic charges for benzene (Table S3) were derived using the R.E.D. Server[10] with the same settings as described for the R_8 and S_5 residues.

Trajectory analysis

For both sets of LMMD simulations, the 10 individual runs were combined into a single trajectory for analysis. Benzene occupancy grids were generated using the ptraj module of AMBER 11 to bin carbon atoms of benzenes into 1 Å × 1 Å × 1 Å grid cells. The cutoff isocontour value used for visualization of benzene occupancy was five times the threshold bulk value, which was defined as the highest isovalue at which benzenes were detected in the bulk solvent. This is an arbitrary criterion that serves to filter out most of the spurious binding sites, leaving behind those that are likely to be legitimate. In order to compare the overlap of the benzene occupancy maps with known MDM2 ligands, the respective ligand-bound

MDM2 structures were aligned using PyMOL[18] to the average protein structure sampled during the LMMD simulations.

Peptide design

A suitable structural snapshot, in which the second nutlin interaction site bound a benzene molecule, was selected from each of the two sets of LMMD simulations performed on unbound and p53-bound MDM2. The structure with the most deeply buried benzene was chosen, and this was determined by measuring the distance between the benzene's centre of mass and Cγ of Leu107, which forms the base of the pocket. Care was taken to ensure that the side-chain torsion angle $\chi 1$ of Tyr100 in the selected structures was less than -170° to avoid steric clashes with the peptide backbone.

The p53 peptide (ETFSDLWKLLPEN) was modeled onto the selected unbound MDM2 structure by extraction from the 1YCR crystal structure, following superimposition of the two protein structures. A phenylalanine residue was appended to the peptide's C-terminus using PyMOL,[18] such that there was optimal overlap of the phenyl group with the benzene molecule bound at the second nutlin interaction site. The C-terminal phenylalanine was added in the same way to the peptide in the selected p53-bound MDM2 structure. These extended p53 peptides were subsequently mutated to match the sequence of the sMTide-02 peptide, except that an i, $i + 4$ staple with an R,R configuration was introduced instead of an i, $i + 7$ staple, by using the LEaP module of AMBER 11 to add the side chains of the mutated residues and form the cis carbon-carbon double bond between two R_5 residues, keeping the peptide backbone fixed. R_5 represents an (R)-2-(4'-pentenyl)alanine residue. Analogous stapled peptides with tyrosine instead of phenylalanine at the C-terminus were similarly modeled. These new stapled peptides were named YS-1 (TSF**R$_5$**EYW**R$_5$**LLPENF) and YS-2 (TSF**R$_5$**EYW**R$_5$**LLPENY) respectively.

The four modeled stapled peptide complexes (two from unbound MDM2, and two from p53-bound MDM2) were each subject to explicit-solvent MD simulations for 50 ns. The ff99SB-ILDN and GAFF force fields were used to describe the R_5 residues during the simulations. Atomic charges for R_5 (Table S4) were derived using the R.E.D. Server as described earlier for the R_8 and S_5 residues. All peptides were capped by acetyl and amide groups.

Binding free energy calculations

Binding free energies for MDM2 complexes with wild-type (WT) p53 peptide, sMTide-02 and the two designed stapled peptides YS-1 and YS-2 (Table S5), were calculated using the molecular mechanics/generalized Born surface area (MM/GBSA) method,[19] in which the free energies of the complex (G_{com}), receptor (G_{rec}) and ligand (G_{lig}) are calculated individually and the free energy of binding (ΔG_{bind}) obtained as follows:

$$\Delta G_{bind} = G_{com} - G_{rec} - G_{lig}$$
$$= \Delta E_{MM} + \Delta G_{sol} - T\Delta S \qquad (1)$$

ΔG_{bind} is evaluated as the sum of the changes in the molecular mechanical energies (ΔE_{MM}), which includes van der Waals (ΔE_{vdw}), electrostatic (ΔE_{ele}) and internal energies (ΔE_{int}), solvation free energies (ΔG_{sol}), which includes polar (ΔG_{GB}) and nonpolar contributions (ΔG_{np}), and entropy ($-T\Delta S$).

$$\Delta E_{MM} = \Delta E_{vdw} + \Delta E_{ele} + \Delta E_{int} \qquad (2)$$

$$\Delta G_{sol} = \Delta G_{GB} + \Delta G_{np} \qquad (3)$$

$$G_{np} = \gamma \times SASA + \beta \qquad (4)$$

All programs used for MM/GBSA calculations are from AMBER 11. 200 equally-spaced snapshot structures were extracted from the last 20-40 ns of each of the trajectories, depending on when equilibration of the systems occurred (indicated by plateauing of their root-mean-square deviation [RMSD] plots), and their molecular mechanical energies calculated with the sander module. The polar contribution to the solvation free energy (ΔG_{GB}) was calculated by the pbsa[20] program using the modified generalized Born (GB) model described by Onufriev et al.[21] while the nonpolar contribution (ΔG_{np}) was estimated from the solvent accessible surface area (SASA) using the molsurf[22] program with $\gamma = 0.0072$ kcal Å^{-2} and β set to zero. Entropies were estimated by normal mode analysis[23] using the nmode program. Due to its computational expense, only 50 equally-spaced snapshots from the equilibrated portion of the trajectories were used for entropic analysis.

2. Peptide synthesis

Ramage Chemmatrix resin was obtained from PCAS-Biomatrix (Quebec, Canada). L-amino acids were obtained from Advanced Chemtech (Louisville, KY). Fmoc-threonine, serine, glutamic acid and tyrosine were t-butyl protected and Fmoc-tryptophan was not Boc protected. Unnatural alkenyl amino acids were purchased from OKeanos (Beijing, China). All other solvents and reagents were obtained from Sigma-Aldrich. 1,2-dichloroethane (DCE) was dried overnight over activated molecular sieves and purged with argon for 30 min prior to use. All other reagents were used as received.

The peptides were synthesized by Fmoc chemistry on a Syro II peptide synthesizer (Biotage) at the 0.1 mmol scale using Ramage Chemmatrix resin (0.53 mmol/g). The dry resin was swelled with N-methyl-2-pyrrolidinone (NMP) before use. The Fmoc protecting group was removed by treatment with 40% piperidine in NMP (3 min) followed by a second treatment with 20% piperidine in NMP (12 min). The Fmoc-protected amino acids (5 equiv.) were coupled using N,N'-diisopropylcarbodiimide (DIC) as the activating agent (5 equiv.) and 1-hydroxy-7-azabenzotriazole (HOAt) as the additive in NMP (0.5 M). The coupling time was 90 min for all amino acids except for (R)-2-(4′-pentenyl)alanine, (S)-N-Fmoc-2-(4'-pentenyl)alanine and (R)-N-Fmoc-2-(7'-octenyl)alanine (**R$_5$**, **S$_5$** and **R$_8$** respectively). **R$_5$**, **S$_5$** and **R$_8$** (4 equiv.) were manually pre-activated for 7 min and coupled to the peptide resin for two hours. Following deprotection of the final Fmoc group, the peptides were acetylated using a mixture of acetic anhydride/diisopropylethylamine/dimethylformamide (2/2/1) for 60 min. After each coupling, deprotection and acetylation reaction, the resin was thoroughly washed with NMP.

Ring-closing metathesis of resin-bound, N-acetylated peptides was performed manually using a 5 mg/mL solution of Grubbs I catalyst (20 mol%) in dry DCE at room temperature under an atmosphere of inert argon (3 x 2 h treatments). After the reaction, the solution was drained, the resin washed with DCE (3 x 1 min), dimethyl sulfoxide (1 x 2 h) and methanol (3 x 1 min) then dried *in vacuo* overnight. Cleavage of the peptide from the resin was achieved using 8 mL of a cocktail of trifluoroacetic acid/triisopropylsilane/water (95/2.5/2.5) for 2 h followed by filtration and precipitation with diethyl ether. The

precipitate was collected by centrifugation, dried and redissolved in a 3:2 mixture of acetonitrile and water.

The pure peptides (>90% purity) were obtained by purification using a preparative high-performance liquid chromatography (HPLC) system (Agilent) on a Jupiter C12 reversed-phase preparative column (Phenomenex, 4 μm, Proteo 90 Å, 250 x 10 mm). The peptides were characterized by liquid chromatography-mass spectrometry (LC-MS). Mass spectra were obtained by electrospray in negative ion mode. A representative LC trace and mass spectrum are shown in Figure S2. The mass spectral data for all the synthesized peptides are summarized in Table S6.

3. Biophysical assays

Protein purification for fluorescence polarization experiments

MDM2 (1–125) was ligated into the GST fusion expression vector pGEX-6P-1 (GE Lifesciences) via a BAMH1 and NDE1 double digest. BL21(DE3) competent *Escherichia coli* were then transformed with the GST-tagged MDM2 construct (1–125). The cells expressing the MDM2 GST fusion construct were grown in LB medium at 37 °C overnight to an OD_{600} of ~0.6 and induction was carried out with 1 mM isopropyl-beta-D-thiogalactopyranoside (IPTG) at room temperature. Cells were harvested by centrifugation and the cell pellets were resuspended in 50 mM Tris pH 8.0, 10% sucrose and then sonicated. The sonicated sample was centrifuged for 60 min at 17,000 g at 4 °C. The supernatant was applied to a 5 ml FF GST column (Amersham) pre-equilibrated in wash buffer (phosphate buffered saline [PBS], 2.7 mM KCl and 137 mM NaCl, pH 7.4) with 1 mM dithiothreitol (DTT). The column was then further washed with six volumes of wash buffer. MDM2 was then purified from the column by cleavage with PreScission (GE Lifesciences) protease. 10 units of PreScission protease, in one column volume of PBS with 1 mM DTT buffer, were injected onto the column. The cleavage reaction was allowed to proceed overnight at 4 °C. The cleaved protein was then eluted from the column with wash buffer. Protein fractions were analyzed with SDS-PAGE and concentrated using a Centricon (3.5 kDa MWCO) concentrator (Millipore). The MDM2 protein sample was then dialyzed into a buffer solution containing 20 mM Bis-Tris, pH 6.5, 50 mM NaCl with 1 mM DTT and loaded onto a monoS column pre-equilibrated in buffer A (20 mM Bis-Tris, pH 6.5, 1 mM DTT). The column was then washed in six column volumes of buffer A and bound protein was eluted with a linear gradient of 1 M NaCl over 25 column volumes. Protein fractions were analyzed with SDS-PAGE and concentrated using a Centricon (3.5 kDa MWCO) concentrator, Millipore. The cleaved MDM2 (1-125) was purified to ~90% purity. Protein concentration was determined using A280 with extinction coefficient of 10430 M^{-1} cm^{-1} for MDM2 (1–125).

Competitive fluorescence polarization assays and K_d determination.

Purified MDM2 (1-125) protein was titrated against 50 nM carboxyfluorescein (FAM)-labeled 12/1 peptide[24] (FAM-RFMDYWEGL-NH$_2$). Dissociation constants for titration of MDM2 against FAM-labeled 12/1 peptide were determined by fitting the experimental data to a 1:1 binding model equation shown below:[25,26]

$$r = r_o + (r_b - r_o) \times \frac{(K_d + [L]_t + [P]_t) - \sqrt{K_d + [L]_t + [P]_t)^2 - 4[L]_t[P]_t}}{2[L]_t} \tag{5}$$

[P] is the protein concentration (MDM2), [L] is the labeled peptide concentration, r is the anisotropy measured, r0 is the anisotropy of the free peptide, r_b is the anisotropy of the MDM2–FAM-labeled peptide complex, K_d is the dissociation constant, $[L]_t$ is the total FAM labeled peptide concentration, and $[P]_t$ is the total MDM2 concentration. The determined apparent K_d value of FAM-labeled 12/1 peptide (13.0 nM) was used to determine the apparent K_d values of the respective competing ligands in subsequent competition assays.

Apparent K_d values were determined for a variety of molecules via competitive fluorescence polarization experiments. Titrations were carried out with the concentration of MDM2 held constant at 250 nM and the labeled peptide at 50 nM. The competing molecules were then titrated against the complex of the FAM-labeled peptide and protein. Apparent K_d values were determined by fitting the experimental data to the equations shown below:[26,27]

$$r = r_o + (r_b + r_o) \times \frac{2\sqrt{(d^2 - 3e)}\cos(\theta/3) - 9}{3K_{d1} + 2\sqrt{(d^2 - 3e)}\cos(\theta/3) - d} \tag{6}$$

$$d = K_{d1} + K_{d2} + [L]_{st} + [L]_t - [P]_t \tag{7}$$

$$e = ([L]_t - [P]_t)K_{d1} + ([L]_{st} - [P]_t)K_{d2} + K_{d1}K_{d2} \tag{8}$$

$$f = -K_{d1}K_{d2}[P]_t \tag{9}$$

$$\theta = ar\cos\left[\frac{-2d^3 + 9de - 27f}{2\sqrt{(d^2 - 3e)^3}}\right] \tag{10}$$

$[L]_{st}$ and $[L]_t$ denote labeled ligand and total unlabeled ligand input concentrations, respectively. K_{d2} is the dissociation constant of the interaction between the unlabeled ligand

and the protein. In all competitive types of experiments, it is assumed that $[P]_t > [L]_{st}$, otherwise considerable amounts of free labeled ligand would always be present and would interfere with measurements. K_{d1} is the apparent K_d for the labeled peptide used in the respective experiment, which has been experimentally determined as described in the previous paragraph. The FAM-labeled peptide was dissolved in dimethyl sulfoxide (DMSO) at 1 mM and diluted into experimental buffer (PBS [10 mM Na_2HPO_4, 2 mM KH_2PO_4, pH 7.4], 2.7 mM KCl, 137 mM NaCl, 0.1% Tween 20). All titrations were carried out in triplicate. Curve-fitting was carried out using Prism 4.0 (GraphPad).

To validate the fitting of a 1:1 binding model we carefully determined that the anisotropy value at the beginning of the direct titrations between MDM2 and the FAM-labeled peptide did not differ significantly from the anisotropy value observed for the free fluorescently labeled peptide. Negative control titrations of the ligands under investigation were also carried out with the fluorescently labeled peptide (in the absence of MDM2) to ensure no interactions were occurring between the ligands and FAM-labeled peptide. In addition, we ensured that the final baseline in the competitive titrations did not fall below the anisotropy value for the free FAM-labeled peptide, which would otherwise indicate an unintended interaction between the ligand and the FAM-labeled peptide to be displaced from the MDM2 binding site.

Circular dichroism
Circular dichroism (CD) spectra were obtained on a Chirascan-plus spectropolarimeter, using a quartz cuvette (Helmer) with a pathlength of 0.1 cm. Far ultraviolet (UV) CD spectra were recorded from 260 nm to 200 nm at a peptide concentration of either 2 mg/ml or 0.5 mg/ml, respectively. Peptides were dissolved in 5 mM sodium phosphate buffer (pH 7.0) containing 30% (v/v) isopropanol. The CD signal was converted into Delta Epsilon ($\Delta\varepsilon$) in units of $M^{-1} \cdot cm^{-1}$ and plotted. CD spectra were recorded at a data pitch of 0.2 nm at 50 nm/min, a response time of 2 s, and a bandwidth of 2 nm.

4. X-ray crystallography

Protein purification

MDM2 17-125 E69AK70A was cloned into the pGEX6P-1 plasmid (GE Healthcare) with an N-terminal GST fusion and expressed in BL21(DE3)pLysS *E. coli*. The cells were grown in LB media at 37 ˚C until an OD_{600} of 0.6, induced with 0.2 mM IPTG and incubated overnight at 20 ˚C. The cells were harvested by centrifugation (4000 × g, 4 °C, 20 min) and then the cell pellets were resuspended in buffer B (20 mM HEPES pH 7.4, 100 mM NaCl, 5 mM DTT) supplemented with 250 µg/ml lysozyme, 50 µg/ml RNase A, 10 µg/ml DNase I and 5 mM $MgCl_2$. The cells were lysed by sonication and the lysate cleared by centrifugation (50,000 x g, 4 ˚C, 1 hr). The supernatant was incubated with glutathione resin (GE Healthcare) overnight followed by washing with buffer B and elution with buffer B supplemented with 20 mM glutathione. The GST fusion protein was removed with PreScission 3C protease and the sample was then loaded onto a Superdex 75 26/60 gel filtration column (GE Healthcare) equilibrated in buffer B. Purified monomeric MDM2 17-125 E69AK70A was diluted to 0.5 mg/ml and incubated with YS-1 or YS-2 at a 1:1.1 molar ratio overnight at 4 ˚C. Both complexes were concentrated to 5 mg/ml for crystallization.

Structure determination

Crystals of MDM2 in complex with YS-1 were grown at 4 °C in a solution of 0.1 M sodium citrate pH 4.2, 0.2 M NaCl and 20% PEG8000. These crystals were used for data collection for the MDM2–YS-1 structure and for seeding into MDM2–YS-2 trays. The seeds were produced using a Seed Bead (Hampton Research) according to the manufacturer's instructions and then combined with MDM2-YS-2 and a precipitant of 0.1 M sodium citrate pH 4.0 and 15% PEG8000 at a ratio of 1:3:2. Both the YS-1 and the YS-2 crystals were cryoprotected in reservoir solution supplemented with 20% PEG400 and flash cooled in liquid nitrogen. Diffraction data were collected on single crystals at 100 K on beamline I04 (YS-1) and beamline I04-1 (YS-2) at Diamond Light Source. The data were processed with xia2[28] and then re-processed with Aimless[29] and Pointless[30] in CCP4i.[31] Molecular replacement was performed with Phaser[32] and the models were refined using cycles of refinement with Refmac[33] and manual correction in Coot.[34] The final models were validated with MolProbity.[35] Data collection and refinement statistics are presented in Table S7. The

coordinates were deposited in the PDB under the accession codes 4UE1 and 4UD7 (YS-1 and YS-2 respectively).

5. Additional MD simulations

MDM2 (residues 17-111) bound to YS-1

In the crystal structures of both MDM2–YS-1 and MDM2–YS-2, chains A and B of MDM2 undergo N-terminal strand exchange (Figure S4). This strand exchange is not observed for chains C and D of MDM2. Multiple MD simulations of a strand exchange dimer in the crystal structure of the MDM2–YS-1 complex were carried out to investigate this phenomenon.

Chains A and F of the crystal structure of MDM2 bound to YS-1 (PDB code 4UE1) were used to initiate the simulations. The N-terminal cloning artifact sequence GPLGS was removed from chain A. All crystallographic waters within 4 Å of the selected chains were retained, while the double MDM2 mutations, E69A and K70A, were reverted to their wild type status. Acetyl and N-methyl groups were used to cap the N- and C- termini of MDM2 respectively. Three independent 100-ns MD simulations of the MDM2–YS-1 complex were performed using the same settings and protocol as described earlier for the other MDM2 complexes.

In all three simulations, the MDM2 N-terminal lid (residues 17-24) was unambiguously observed to fold back over the second nutlin interaction site towards the domain core, forming a cradle around Phe30 (Figure S8), which remained bound to the proximal P27 site. This is similar to the packing of the N-terminal lid from chain B against α4 of chain A observed in the crystal structures, suggesting that the proximal P27 site is indeed a functional ligand-binding site that is defined by residues from the MDM2 N-terminal core domain and N-terminal lid. Thus, the improved binding affinity of YS-1 and YS-2 over the control peptide YS-3 could be attributed to the interaction of Phe/Tyr30 with the proximal P27 site.

MDM2 (residues 25-109) bound to YS-1 and YS-2

To obtain comparable free energy values with those derived from the simulations initiated with the 1YCR PDB structure, the N- and C- termini of MDM2 in the crystal structures of its complexes with YS-1 (PDB code 4UE1) and YS-2 (PDB code 4UD7) were truncated, leaving residues 25-109. Each of these modified complexes, with the peptides bound at the proximal

P27 site, were subjected to two independent 50-ns MD simulations followed by MM/GBSA analysis (Table S5), using the same settings and protocol as described above.

6. Supplementary tables

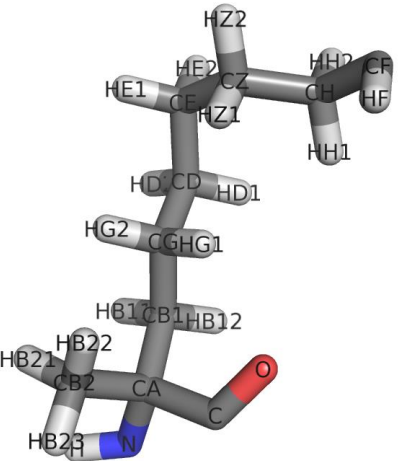**Table S1.** Parameters of (*R*)-2-(7'-octenyl)alanine fragment (**R₈**).

	Atom names	GAFF/AMBER atom type	Partial charge
	N	N	-0.4157
	H	H	0.2719
	C	C	0.5973
	O	O	-0.5679
	CA	CT	-0.0101
	CB1	CT	0.0867
	HB11, HB12	HC	0.0161
	CB2	CT	-0.0629
	HB21, HB22, HB23	HC	0.0160
	CG	CT	-0.0274
	HG1, HG2	HC	0.0520
	CD	CT	-0.1354
	HD1, HD2	HC	0.0292
	CE	CT	0.0101
	HE1, HE2	HC	-0.0077
	CZ	CT	0.0668
	HZ1, HZ2	HC	-0.0164
	CH	CT	0.0130
	HH1, HH2	HC	0.0354
	CF	c2	-0.2596
	HF	hc	0.1680

Table S2. Parameters of (*S*)-2-(4'-pentenyl)alanine fragment (**S₅**).
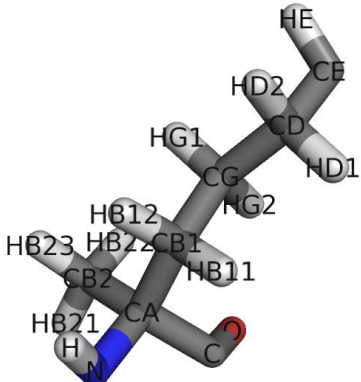
	Atom names	GAFF/AMBER atom type	Partial charge
	N	N	-0.4157
	H	H	0.2719
	C	C	0.5973
	O	O	-0.5679
	CA	CT	0.0335
	CB1	CT	-0.1254
	HB11, HB12	HC	0.0371
	CB2	CT	-0.0414
	HB21, HB22, HB23	HC	0.0351
	CG	CT	0.0092
	HG1, HG2	HC	0.0310
	CD	CT	0.0559
	HD1, HD2	HC	0.0190
	CE	c2	-0.2280
	HE	hc	0.1291

Table S3. Parameters of benzene.
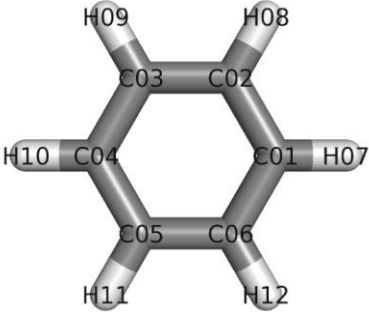
	Atom names	GAFF atom type	Partial charge
	C01, C02, C03, C04, C05, C06	ca	-0.1259
	H07, H08, H09, H10, H11, H12	ha	0.1259

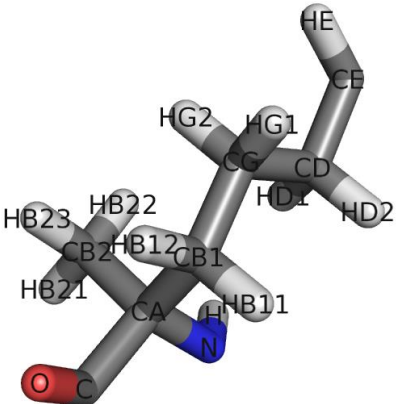**Table S4.** Parameters of (*R*)-2-(4'-pentenyl)alanine fragment (**R₅**).

	Atom names	GAFF/AMBER atom type	Partial charge
	N	N	-0.4157
	H	H	0.2719
	C	C	0.5973
	O	O	-0.5679
	CA	CT	0.0518
	CB1	CT	0.0271
	HB11, HB12	HC	0.0212
	CB2	CT	-0.3729
	HB21, HB22, HB23	HC	0.1128
	CG	CT	0.0662
	HG1, HG2	HC	-0.0002
	CD	CT	0.0134
	HD1, HD2	HC	0.0287
	CE	c2	-0.2311
	HE	hc	0.1221

Table S5. Computed binding free energy components (kcal/mol) of MDM2 peptide ligands.

Peptide	Sequence	ΔH	TΔS	ΔG
wild-type p53	Ac-^{17}ETFSDLWKLLPEN^{29}-NH$_2$	-56.8 ± 0.9	-44.1 ± 2.9	-12.7 ± 3.8
sMTide-02	Ac-^{17}TSF**R$_8$**EYWALL**S$_5$**^{27}-NH$_2$	-57.0 ± 1.6	-34.1 ± 3.1	-22.8 ± 1.5
YS-1 (bound to second nutlin site)	Ac-^{17}TSF**R$_5$**EYW**R$_5$**LLPENF^{30}-NH$_2$	-80.7 ± 2.3	-49.0 ± 0.1	-31.7 ± 2.3
YS-2 (bound to second nutlin site	Ac-^{17}TSF**R$_5$**EYW**R$_5$**LLPENY^{30}-NH$_2$	-81.8 ± 0.5	-48.0 ± 0.9	-33.9 ± 1.4
YS-1 (bound to P27 site)	Ac-^{17}TSF**R$_5$**EYW**R$_5$**LLPENF^{30}-NH$_2$	-71.9 ± 2.0	-45.7 ± 5.6	-26.2 ± 3.7
YS-2 (bound to P27 site)	Ac-^{17}TSF**R$_5$**EYW**R$_5$**LLPENY^{30}-NH$_2$	-72.7 ± 0.4	-46.6 ± 1.0	-26.2 ± 1.4

Table S6. Mass spectrometry data for the stapled peptides described in this study.

Peptide	Calculated Mass	Found Mass	ESI ion mode
sMTide-02	1462.75	1461.62 [M – H]	negative
YS-1	1837.11	1836.16 [M – H]	negative
YS-2	1853.11	1852.16 [M – H]	negative
YS-3	1688.85	1688.32 [M – H]	negative
YS-4	1761.01	1760.28 [M – H]	negative
YS-5	1827.07	1826.05 [M – H]	negative
YS-6	1843.07	1842.40 [M – H]	negative

Table S7. Data collection and refinement statistics. Statistics for the highest resolution shell are included in parentheses.

| Data collection	MDM2/YS-1	MDM2/YS-2
Wavelength (Å)	0.979	0.920
Space group	P 1 2_1 1	P 1 2_1 1
a, b, c (Å)	46.1, 69.5, 78.6	46.1, 69.5, 78.5
α, β, γ (˚)	90.0, 102.0, 90.0	90.0, 102.4, 90.0
Resolution	51.53-1.45 (1.47-1.45)	51.50-1.60 (1.63-1.60)
Observed reflections	291085 (7823)	231790 (9656)
Unique reflections	84267 (3582)	62522 (2945)
I/σ(I)	16.1 (1.7)	12.1 (1.9)
R_{merge}	0.033 (0.577)	0.055 (0.693)
Multiplicity	3.5 (2.2)	3.7 (3.3)
Completeness	98.1 (84.4)	97.9 (93.9)
Refinement		
R/R_{free} (%)	16.5 / 20.0	13.9 / 17.8
Rmsd bond lengths (Å)	0.025	0.011
Rmsd bond angles (˚)	2.68	1.48

7. Supplementary figures
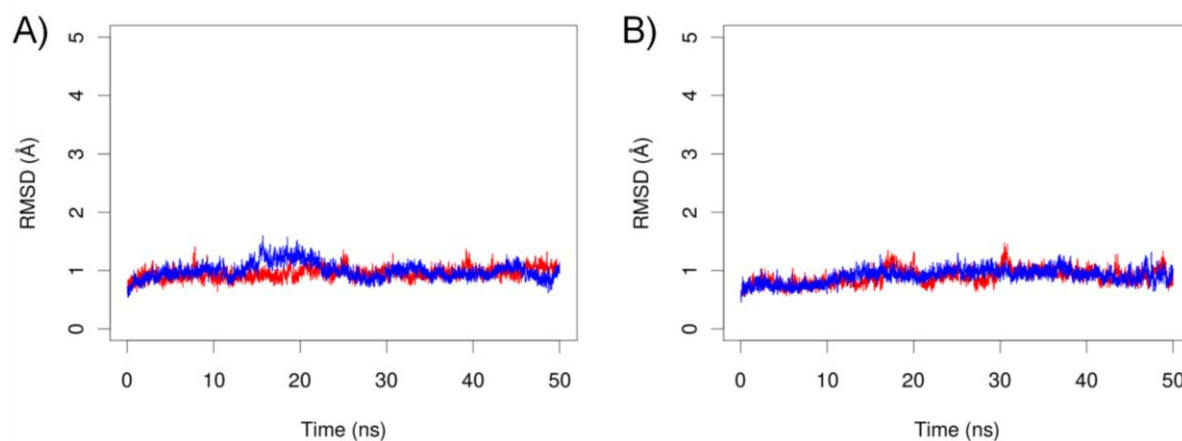
Figure S1. Cα RMSD of MDM2 complexes with (A) YS-1 and (B) YS-2 during 50-ns MD simulations. Two different initial structures obtained from the apo (red) and holo (blue) LMMD simulations were used to simulate each complex.
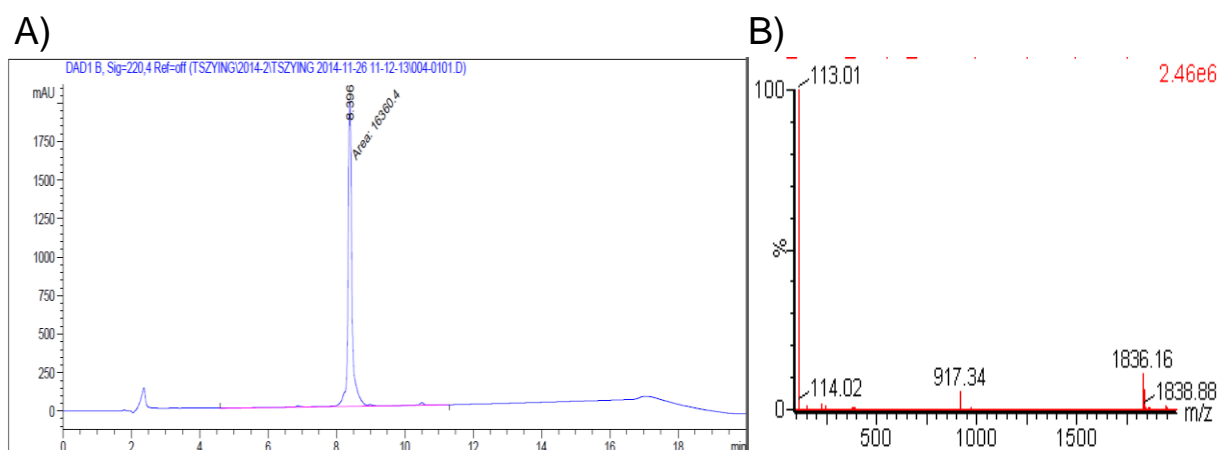
Figure S2. LC-MS trace from purified peptide YS-1 as a representative example (Agilent 1260 instrument, Jupiter C12 column). (A) LC chromatograph of peptide YS-1. (B) Electrospray mass spectrum (negative ion mode) of peptide YS-1.
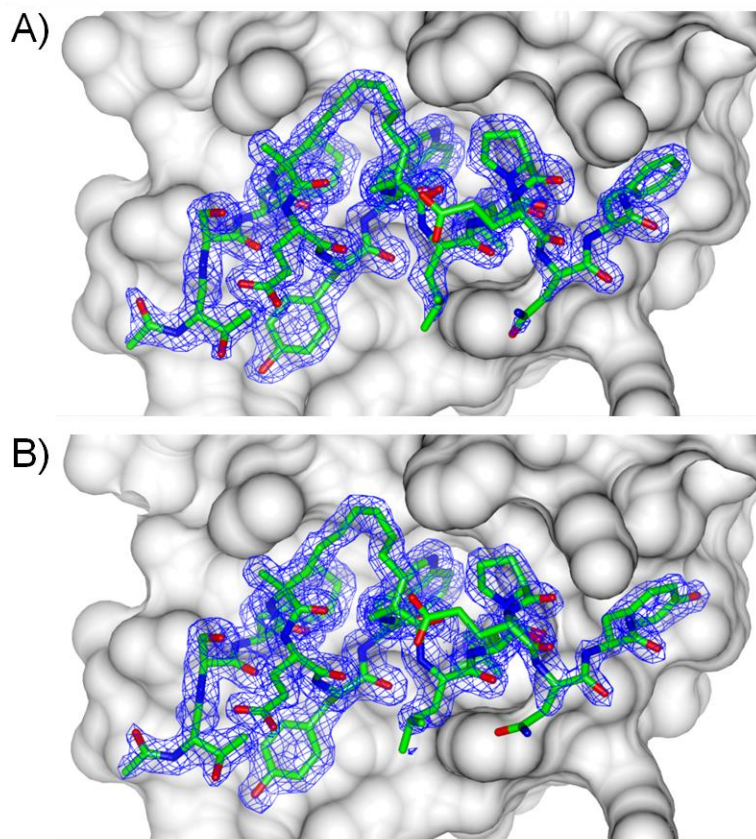
Figure S3. 2Fo-Fc electron density maps of the stapled peptides. The maps are shown for (A) YS-1 and (B) YS-2 and are contoured at 1.3 σ. Chains A (protein) and F (peptide) are shown in both figures. Good density was observed across both stapled peptides, with the exception of the side chains of Glu28 and Asn29, which exhibited limited density.
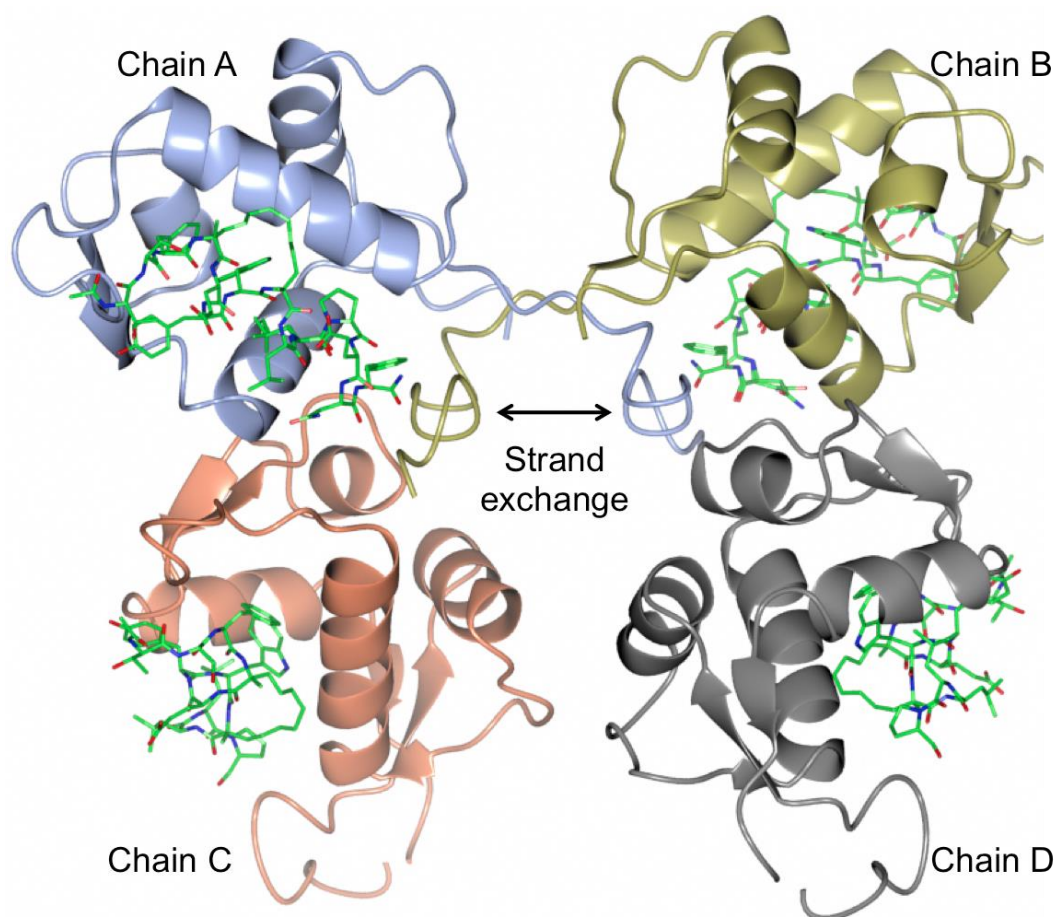
Figure S4. The asymmetric unit of the structure of MDM2–YS-1, highlighting the strand exchange between chains A and B. This exchange cannot occur in chains C and D due to crystal contacts.
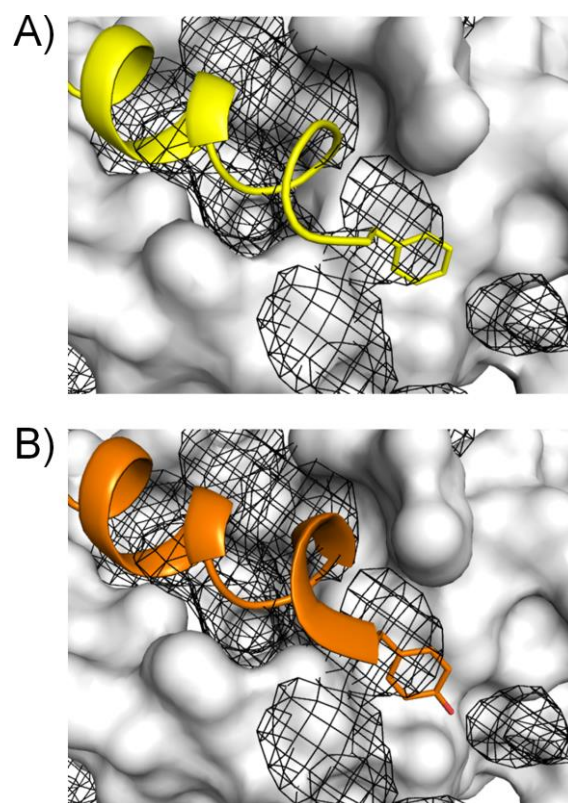
Figure S5. Benzene occupancy maps (black mesh) of MDM2 superimposed on the crystal structures of MDM2 (white) in complex with (A) YS-1 (yellow) and (B) YS-2 (orange). The cutoff isocontour value used for visualization of benzene occupancy here is four times the threshold bulk value.
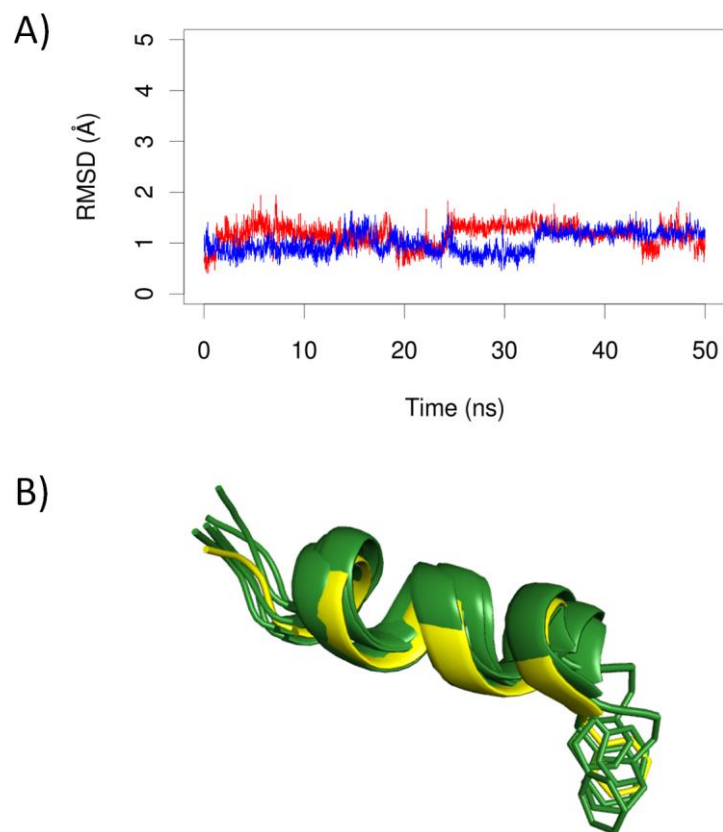
Figure S6. Stability of crystallographic binding mode of YS stapled peptides in MD simulations. (A) Backbone RMSD of YS-1 (red) and YS-2 (blue) peptides from their respective crystallographic conformations. (B) Superposition of five MD snapshots of YS-1 (green) with the crystallographic conformation of YS-1 (yellow) in its complex with MDM2.
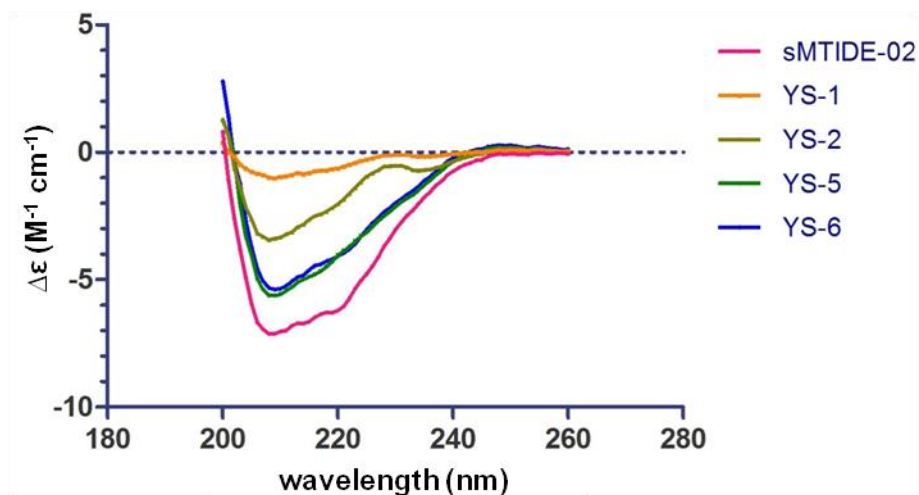
Figure S7. Circular dichroism spectra of stapled peptides. The free energy of forming the α-helical structure for the proline-containing peptides YS-1 and YS-2 is estimated to be in the range of 1.5–2.0 kcal/mol, using the formula $\Delta G = -RT\ln K$, where K is the ratio of the population of folded peptide to the population of unfolded peptide.
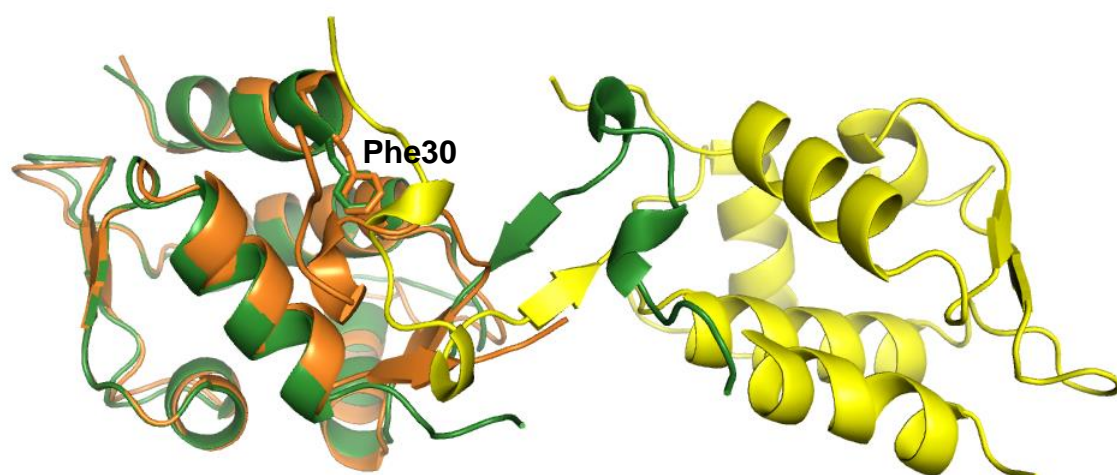
Figure S8. Comparison of an MDM2–YS-1 complex trajectory structure (orange) at the end of a 100-ns MD simulation with the strand exchange dimer (green and yellow) in the crystal structure. The MDM2 N-terminal lids of both the trajectory structure and strand exchange partner (yellow) are shown to cradle Phe30 (stick form) of YS-1.

8. References

(1)   Berman, H. M.; Westbrook, J.; Feng, Z.; Gilliland, G.; Bhat, T. N.; Weissig, H.; Shindyalov, I. N.; Bourne, P. E. The Protein Data Bank. *Nucleic Acids Res.* **2000**, *28*, 235-242.

(2)   Kussie, P. H.; Gorina, S.; Marechal, V.; Elenbaas, B.; Moreau, J.; Levine, A. J.; Pavletich, N. P. Structure of the MDM2 Oncoprotein Bound to the p53 Tumor Suppressor Transactivation Domain. *Science* **1996**, *274*, 948-953.

(3)   Pazgier, M.; Liu, M.; Zou, G.; Yuan, W.; Li, C.; Li, C.; Li, J.; Monbo, J.; Zella, D.; Tarasov, S. G.; Lu, W. Structural Basis for High-Affinity Peptide Inhibition of p53 Interactions with MDM2 and MDMX. *Proc. Natl. Acad. Sci. U. S. A.* **2009**, *106*, 4665-4670.

(4)   Brown, C. J.; Quah, S. T.; Jong, J.; Goh, A. M.; Chiam, P. C.; Khoo, K. H.; Choong, M. L.; Lee, M. A.; Yurlova, L.; Zolghadr, K.; Joseph, T. L.; Verma, C. S.; Lane, D. P. Stapled Peptides with Improved Potency and Specificity That Activate p53. *ACS Chem. Biol.* **2013**, *8*, 506-512.

(5)   Case, D. A.; Darden, T. A.; Cheatham, T. E.; Simmerling, C. L.; Wang, J.; Duke, R. E.; Luo, R.; Walker, R. C.; Zhang, W.; Merz, K. M.; Roberts, B.; Wang, B.; Hayik, S.; Roitberg, A.; Seabra, G.; Kolossvái, I.; Wong, K. F.; Paesani, F.; Vanicek, J.; Liu, J.; Wu, X.; Brozell, S. R.; Steinbrecher, T.; Gohlke, H.; Cai, Q.; Ye, X.; Wang, J.; Hsieh, M.-J.; Cui, G.; Roe, D. R.; Mathews, D. H.; Seetin, M. G.; Sagui, C.; Babin, V.; Luchko, T.; Gusarov, S.; Kovalenko, A.; Kollman, P. A. *Amber 11*, University of California, San Francisco, 2010.

(6)   Dolinsky, T. J.; Czodrowski, P.; Li, H.; Nielsen, J. E.; Jensen, J. H.; Klebe, G.; Baker, N. A. PDB2PQR: Expanding and Upgrading Automated Preparation of Biomolecular Structures for Molecular Simulations. *Nucleic Acids Res.* **2007**, *35*, W522-W525.

(7)   Jorgensen, W. L.; Chandrasekhar, J.; Madura, J. D.; Impey, R. W.; Klein, M. L. Comparison of Simple Potential Functions for Simulating Liquid Water. *J. Chem. Phys.* **1983**, *79*, 926-935.

(8)   Lindorff-Larsen, K.; Piana, S.; Palmo, K.; Maragakis, P.; Klepeis, J. L.; Dror, R. O.; Shaw, D. E. Improved Side-Chain Torsion Potentials for the Amber ff99SB Protein Force Field. *Proteins: Struct. Funct. Bioinform.* **2010**, *78*, 1950-1958.

(9)   Wang, J. M.; Wolf, R. M.; Caldwell, J. W.; Kollman, P. A.; Case, D. A. Development and Testing of a General Amber Force Field. *J. Comput. Chem.* **2004**, *25*, 1157-1174.

(10)   Vanquelef, E.; Simon, S.; Marquant, G.; Garcia, E.; Klimerak, G.; Delepine, J. C.; Cieplak, P.; Dupradeau, F.-Y. R.E.D. Server: A Web Service for Deriving RESP and ESP Charges and Building Force Field Libraries for New Molecules and Molecular Fragments. *Nucleic Acids Res.* **2011**, *39*, W511-W517.

(11)   Cornell, W. D.; Cieplak, P.; Bayly, C. I.; Kollman, P. A. Application of RESP Charges to Calculate Conformational Energies, Hydrogen Bond Energies, and Free Energies of Solvation. *J. Am. Chem. Soc.* **1993**, *115*, 9620-9631.

(12)   Frisch, M. J.; Trucks, G. W.; Schlegel, H. B.; Scuseria, G. E.; Robb, M. A.; Cheeseman, J. R.; Scalmani, G.; Barone, V.; Mennucci, B.; Petersson, G. A.; Nakatsuji, H.; Caricato, M.; Li, X.; Hratchian, H. P.; Izmaylov, A. F.; Bloino, J.; Zheng, G.; Sonnenberg, J. L.; Hada, M.; Ehara, M.; Toyota, K.; Fukuda, R.; Hasegawa, J.; Ishida, M.; Nakajima, T.; Honda, Y.; Kitao, O.; Nakai, H.; Vreven, T.; Montgomery, J., J. A.; Peralta, J. E.; Ogliaro, F.; Bearpark, M.; Heyd, J. J.; Brothers, E.; Kudin, K. N.; Staroverov, V. N.; Kobayashi, R.; Normand, J.; Raghavachari, K.; Rendell, A.; Burant, J. C.; Iyengar, S. S.; Tomasi, J.; Cossi, M.; Rega, N.; Millam, N. J.; Klene, M.; Knox, J. E.; Cross, J. B.; Bakken, V.; Adamo, C.; Jaramillo, J.; Gomperts, R.; Stratmann, R. E.; Yazyev, O.; Austin, A. J.; Cammi, R.; Pomelli, C.; Ochterski, J. W.; Martin, R. L.; Morokuma, K.; Zakrzewski, V. G.; Voth, G. A.; Salvador, P.; Dannenberg, J. J.; Dapprich, S.; Daniels, A. D.; Farkas, Ö.; Foresman, J. B.; Ortiz, J. V.; Cioslowski, J.; Fox, D. J. *Gaussian 09, Revision B.1*, Gaussian, Inc., 2009.

(13)   Ryckaert, J. P.; Ciccotti, G.; Berendsen, H. J. C. Numerical Integration of the Cartesian Equations of Motion of a System with Constraints: Molecular Dynamics of n-Alkanes. *J. Comput. Phys.* **1977**, *23*, 327-341.

(14)   Darden, T.; York, D.; Pedersen, L. Particle Mesh Ewald: An N•Log(N) Method for Ewald Sums in Large Systems. *J. Chem. Phys.* **1993**, *98*, 10089-10092.

(15)   Izaguirre, J. A.; Catarello, D. P.; Wozniak, J. M.; Skeel, R. D. Langevin Stabilization of Molecular Dynamics. *J. Chem. Phys.* **2001**, *114*, 2090-2098.

(16)   Berendsen, H. J. C.; Postma, J. P. M.; Vangunsteren, W. F.; Dinola, A.; Haak, J. R. Molecular Dynamics with Coupling to an External Bath. *J. Chem. Phys.* **1984**, *81*, 3684-3690.

(17) Martinez, L.; Andrade, R.; Birgin, E. G.; Martinez, J. M. Packmol: A Package for Building Initial Configurations for Molecular Dynamics Simulations. *J. Comput. Chem.* **2009**, *30*, 2157-2164.

(18) DeLano, W. L. *The PyMOL Molecular Graphics System*, DeLano Scientific, 2002.

(19) Srinivasan, J.; Cheatham, T. E.; Cieplak, P.; Kollman, P. A.; Case, D. A. Continuum Solvent Studies of the Stability of DNA, RNA, and Phosphoramidate−DNA Helices. *J. Am. Chem. Soc.* **1998**, *120*, 9401-9409.

(20) Luo, R.; David, L.; Gilson, M. K. Accelerated Poisson-Boltzmann Calculations for Static and Dynamic Systems. *J. Comput. Chem.* **2002**, *23*, 1244-1253.

(21) Onufriev, A.; Bashford, D.; Case, D. A. Exploring Protein Native States and Large-Scale Conformational Changes with a Modified Generalized Born Model. *Proteins: Struct. Funct. Bioinform.* **2004**, *55*, 383-394.

(22) Connolly, M. L. Analytical Molecular Surface Calculation. *J. Appl. Crystallogr.* **1983**, *16*, 548-558.

(23) Brooks, B. R.; Janezic, D.; Karplus, M. Harmonic Analysis of Large Systems. I. Methodology. *J. Comput. Chem.* **1995**, *16*, 1522-1542.

(24) Bottger, V.; Bottger, A.; Howard, S. F.; Picksley, S. M.; Chene, P.; GarciaEcheverria, C.; Hochkeppel, H. K.; Lane, D. P. Identification of Novel Mdm2 Binding Peptides by Phage Display. *Oncogene* **1996**, *13*, 2141-2147.

(25) Lai, Z.; Auger, K. R.; Manubay, C. M.; Copeland, R. A. Thermodynamics of p53 Binding to hdm2(1−126): Effects of Phosphorylation and p53 Peptide Length. *Arch. Biochem. Biophys.* **2000**, *381*, 278-284.

(26) Roehrl, M. H. A.; Wang, J. Y.; Wagner, G. A General Framework for Development and Data Analysis of Competitive High-Throughput Screens for Small-Molecule Inhibitors of Protein-Protein Interactions by Fluorescence Polarization. *Biochemistry* **2004**, *43*, 16056-16066.

(27) Wang, Z.-X. An Exact Mathematical Expression for Describing Competitive Binding of Two Different Ligands to a Protein Molecule. *FEBS Lett.* **1995**, *360*, 111-114.

(28) Winter, G. Xia2: An Expert System for Macromolecular Crystallography Data Reduction. *J. Appl. Crystallogr.* **2010**, *43*, 186-190.

(29) Evans, P. R.; Murshudov, G. N. How Good Are My Data and What Is the Resolution? *Acta Crystallogr. Sect. D. Biol. Crystallogr.* **2013**, *69*, 1204-1214.

(30) Evans, P. Scaling and Assessment of Data Quality. *Acta Crystallogr. Sect. D. Biol. Crystallogr.* **2006**, *62*, 72-82.

(31) Winn, M. D.; Ballard, C. C.; Cowtan, K. D.; Dodson, E. J.; Emsley, P.; Evans, P. R.; Keegan, R. M.; Krissinel, E. B.; Leslie, A. G. W.; McCoy, A.; McNicholas, S. J.; Murshudov, G. N.; Pannu, N. S.; Potterton, E. A.; Powell, H. R.; Read, R. J.; Vagin, A.; Wilson, K. S. Overview of the CCP4 Suite and Current Developments. *Acta Crystallogr. Sect. D. Biol. Crystallogr.* **2011**, *67*, 235-242.

(32) McCoy, A. J.; Grosse-Kunstleve, R. W.; Adams, P. D.; Winn, M. D.; Storoni, L. C.; Read, R. J. Phaser Crystallographic Software. *J. Appl. Crystallogr.* **2007**, *40*, 658-674.

(33) Murshudov, G. N.; Vagin, A. A.; Dodson, E. J. Refinement of Macromolecular Structures by the Maximum-Likelihood Method. *Acta Crystallogr. Sect. D. Biol. Crystallogr.* **1997**, *53*, 240-255.

(34) Emsley, P.; Lohkamp, B.; Scott, W. G.; Cowtan, K. Features and Development of Coot. *Acta Crystallogr. Sect. D. Biol. Crystallogr.* **2010**, *66*, 486-501.

(35) Chen, V. B.; Arendall, W. B., III; Headd, J. J.; Keedy, D. A.; Immormino, R. M.; Kapral, G. J.; Murray, L. W.; Richardson, J. S.; Richardson, D. C. Molprobity: All-Atom Structure Validation for Macromolecular Crystallography. *Acta Crystallogr. Sect. D. Biol. Crystallogr.* **2010**, *66*, 12-21.